PAN

Opto-Electronics Review

journal homepage: https://journals.pan.pl/opelre

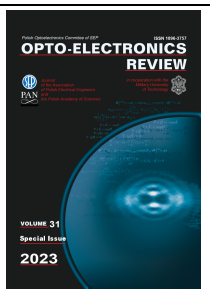

Grating-free high-x InP/$In_xGa_{1-x}As$ mid-wavelength infrared QWIP focal plane array

Cengiz Besikci [1,2*], Saadettin V. Balcı [2], Onur Tanış [1], Oğuz O. Güngör [1], Esra S. Arpaguş [1]

[1]Electrical and Electronics Engineering Department, Middle East Technical University, Dumlupınar Bulvarı 1, 06800 Ankara, Turkey
[2]Micro and Nanotechnology Program, Graduate School of Natural and Applied Sciences, Middle East Technical University, Dumlupınar Bulvarı 1, 06800 Ankara, Turkey

Article info

Article history:
Received 17 Oct. 2022
Received in revised form 07 Dec. 2022
Accepted 18 Dec. 2022
Available on-line 24 Feb. 2023

Keywords:
Infrared imaging; quantum well; infrared photodetector.

Abstract

The authors report the characteristics of a diffraction-grating-free mid-wavelength infrared InP/$In_{0.85}Ga_{0.15}As$ quantum well infrared photodetector focal plane array with a 640 × 512 format and a 15 μm pitch. Combination of a normal incident radiation sensing ability of the high-x $In_xGa_{1-x}As$ quantum wells with a large gain property of the InP barriers led to a diffraction-grating-free quantum well infrared photodetector focal plane array with characteristics displaying great promise to keep the status of the quantum well infrared photodetector as a robust member of the new generation thermal imaging sensor family. The focal plane array exhibited excellent uniformity with noise equivalent temperature difference nonuniformity as low as 10% and a mean noise equivalent temperature difference below 20 mK with f/2 optics at 78 K in the absence of grating. Elimination of the diffraction-grating and large enough conversion efficiency (as high as ~70% at a −3.5 V bias voltage) abolish the bottlenecks of the quantum well infrared photodetector technology for the new generation very small-pitch focal plane arrays.

1. Introduction

New generation thermal imaging sensor technology requires a development of very small-pitch focal plane arrays (FPAs) operating at elevated temperatures with substantial sensitivity and preferable ability for dual/multi-band sensing. While Auger-limited HgCdTe infrared sensors exhibited a successful operation above 77 K, the limited number of suppliers of high-quality CdZnTe substrates and well-known difficulties and high cost of the HgCdTe technology called for the development of alternative technologies mostly based on quantum structured epilayer structures with the motivation to use higher energy bandgap and more robust semiconductors as the detector material. Type-II strained layer superlattice (SLS) technology has shown great potential especially in the mid-wavelength infrared (MWIR) band, and this technology is currently the most widely studied thermal imaging sensor technology.

Quantum well infrared photodetector (QWIP) technology emerged more than two decades ago with great promise as an alternative to HgCdTe. The development of this technology allowed the implementation of large format MWIR and long-wavelength infrared (LWIR) FPAs with desirable performance at relatively long integration times limiting the speed of imaging. However, if the frame time is not limited by the application to allow at least several milliseconds for the integration of the photocurrent, QWIP technology offers a very good performance with excellent uniformity and perfect thermal cycling stability, as well as zero 1/f noise. QWIP technology also provides other important advantages. The typical absorber region of a QWIP pixel is ~1.5 μm thick allowing the implementation of dual/multi-band sensors with no need for deep etching. Another advantage of the QWIPs for dual/multi-band sensor implementation is a relatively narrow spectral response facilitating nearly zero optical crosstalk which is a problem even in small- pitch single band sensors of the alternative technologies [1]. LWIR QWIP FPAs with 15 μm pitch and high performance were reported recently [2].

*Corresponding author at: besikci@metu.edu.tr

https://doi.org/10.24425/opelre.2023.144563
1896-3757/ Association of Polish Electrical Engineers (SEP) and Polish Academic of Sciences (PAS). Published by PAS

An additional advantage of QWIP is the bias adjustable photoconductive gain which can be utilized to maintain temporal coherence in simultaneously integrated dual-band sensors. Therefore, QWIP technology offers indispensable advantages and flexibilities for the new generation thermal imaging systems. However, the extension of these advantages to the very small-pitch sensor technology calls for the elimination of the diffraction grating which exhibits a degraded performance with a decreasing pitch. If this requirement is satisfied, the only drawback of the QWIP technology remains to be the low conversion efficiency (CE = quantum efficiency × gain) inhibiting operation at very low integration times. This bottleneck, which led to the limited success of QWIPs, is associated with the historically incorrect selection of the material systems in the standard MWIR and LWIR QWIP technologies (AlGaAs/GaAs and low-x AlGaAs/$In_xGa_{1-x}As$, respectively). These material systems exhibit almost no ability of normal incident radiation detection calling for diffraction grating and, therefore, a sufficiently large pitch. Even under this condition, the typical quantum efficiency (η) of a standard QWIP pixel is lower than 10%. Furthermore, the QWIPs based on these material systems exhibit a very low pixel conversion efficiency (< 5%) due to the saturation of the photoconductive gain (g) under moderate/large bias voltages (at values typically less than 0.5).

As summarised by the first author in a previous publication [3], there are various articles in the literature reporting higher ability of normal incident radiation detection by quantum wells (QWs) constructed with higher x $In_xGa_{1-x}As$ [4–9]. Normal incident radiation detection ability of these structures was attributed to various reasons such as band mixing effects [7], spin-flip inter-sub band transitions due to strong spin-orbit interaction [5], and higher interface scattering [9]. Maimon *et al.* demonstrated a high-x $In_xGa_{1-x}As$ QWIP on InP substrate with InP/GaInP barriers [10]. Grating-free FPA implementation of a high-x InP/$In_xGa_{1-x}As$ material system with GaInP barriers was also reported recently [11]. The following work [12] implemented in the authors' research laboratory on variable pitch (down to a pixel area of 49 μm^2) grating-free MWIR InP/$In_{0.85}Ga_{0.15}As$ pixel arrays demonstrated desirable performance with ~70% CE and f/2 specific detectivity of ~$1.5\cdot10^{11}$ cmHz$^{1/2}$/W at 78 K at the bias voltages applicable by commercial read-out integrated circuits (ROICs). Furthermore, the characteristics of the pixels including the dark current perfectly scaled with the pixel area exhibiting an advantage over the alternative technologies suffering from pitch reduction problems. The molecular beam epitaxy grown epilayer structure of the InP/$In_{0.85}Ga_{0.15}As$ QWIP included thirty periods of ~35 Å thick $In_{0.85}Ga_{0.15}As$ QW and ~550 Å thick InP barrier with $In_{0.53}Ga_{0.47}As$ top and bottom contacts [12]. The QWs were Si-doped to obtain a 2D electron concentration of ~$5\cdot10^{11}$ cm^{-2}. The epilayer structure was grown on an InP substrate.

In the scope of this work, a 640 × 512 FPA with a 15 μm pitch was fabricated using the above described epilayer structure grown by the first author. This paper reports the characteristics of this diffraction-grating-free MWIR QWIP FPA which exhibited excellent characteristics including a mean noise equivalent temperature difference (NETD) of 24 mK with f/2 optics and a 13 ms integration time (in the absence of anti-reflection coating), and an NETD nonuniformity as low as 10% demonstrating an outstanding pixel uniformity. The desirable performance of the FPA arises from the combination of normal incident radiation sensing ability of the high-x $In_xGa_{1-x}As$ QWs with large gain property of the InP barriers [13] as a solution to the most important bottlenecks of the QWIP technology.

2. Work, results and discussion

The grating-free FPA was fabricated through processes similar to those utilized for the variable pitch pixel arrays whose detailed characteristics were reported earlier [12]. The fabrication procedure included mesa etching, ohmic contact formation, passivation, under-bump metallization, In-coating and lift-off for bump formation, hybridization with a direct injection ROIC and substrate thinning to ~30 μm. Anti-reflection coating was not applied to the FPA. The pixel dimensions of the fabricated FPA were ~12 × 12 μm^2.

Figure 1 shows the normalized spectral responsivity and the peak CE of the variable pitch pixel arrays [12], which should be identical to those of the FPA pixels due to the same epilayer structure and processing conditions used in the fabrication of the FPA and the pixel arrays. The peak responsivity reaches 3 A/W under a −3.5 V bias corresponding to a CE as high as 67% while maintaining an almost bias-independent f/2 specific detectivity of ~$1.5\cdot10^{11}$ cmHz$^{1/2}$/W at 78 K together with a 22% peak quantum efficiency [12]. The sensors did not exhibit 1/f noise down to 1 Hz, and the normalized responsivity did not exhibit any considerable dependence on the bias voltage magnitude and polarity [12].

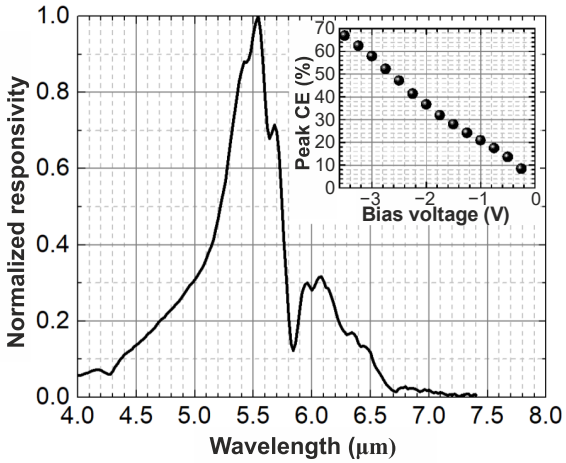

Fig. 1. Normalized spectral responsivity and the peak conversion efficiency of the variable pitch pixel arrays [12].

The dark current and photocurrent density characteristics of the variable pitch pixel arrays [12] are shown in Fig. 2 which do not indicate considerable tunnelling currents down to 78 K. The dark current activation energy is 200 meV which is consistent with the optical activation energy. The sensor is highly background-limited at 78 K with a f/2 aperture under 300 K background.

The FPA was characterised by using a 16-bit imager electronic and a blackbody. Since the maximum reverse

bias voltage applicable by the ROIC was restricted to ~1 V, the characterisation was performed under low bias voltages and sufficiently long integration times (4–30 ms). It should be noted that the FPA should be able to operate at shorter integration times with desirable sensitivity if coupled with an ROIC facilitating higher bias voltages in order to make use of a high pixel CE under this condition.

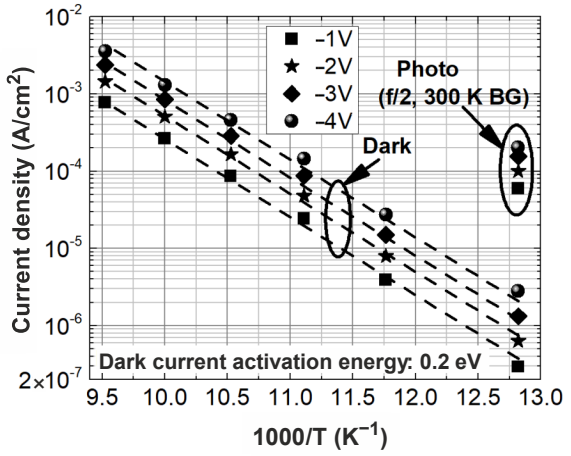

Fig. 2. Dark current and photocurrent density characteristics of the variable pitch pixel arrays [12].

Figure 3 shows the NETD histogram of the operable pixels (NETD < 49 mK) of the FPA with a 13 ms integration time and half-filled ROIC capacitors. The condition for the operability was defined as an NETD below 2 × mean NETD. The operability of the FPA pixels is 99.3%, and the bad pixels are mostly due to fabrication process-oriented defects. The FPA exhibits a truly exceptional NETD nonuniformity of ~10% with the nonuniformity defined as a standard deviation/mean. It should also be noted that this nonuniformity level includes the shading of the cold aperture resulting in nonuniform illumination of the pixels while looking at a uniform target. This NETD nonuniformity is better than that of a typical grating-coupled QWIP, and it is likely that the elimination of diffraction grating improves the responsivity uniformity of the FPA. Unavoidable nonuniformity (from pixel to pixel) in the grating structure of the standard QWIP FPAs is expected to increase the nonuniformity of the FPA due to the strong dependence of the pixel responsivity on the grating-coupling efficiency in these QWIPs with almost no

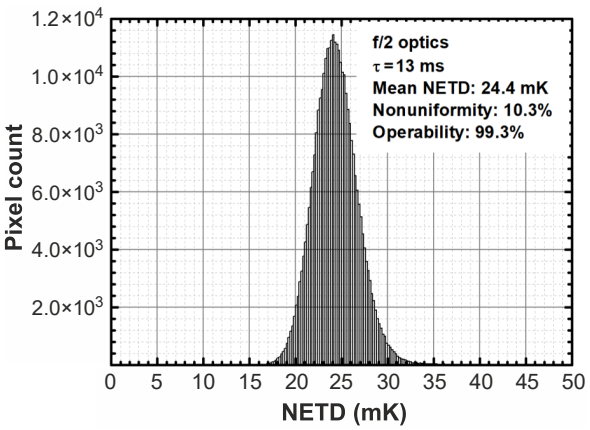

Fig. 3. NETD histogram of the operable pixels at 78 K with a 13 ms integration time and half-filled ROIC capacitors.

ability of normal incident radiation detection. Therefore, removal of the diffraction grating, while eliminating the bottleneck for QWIP pitch reduction, is expected to improve the responsivity and NETD uniformities of the FPA leading to the improved spatial NETD.

In the absence of anti-reflection coating, the FPA exhibits a mean NETD as low as ~24 mK with f/2 optics, 13 ms integration time (τ), and half-filled ROIC capacitors when looking at a 300 K background. Approximately 20% decrease in the NETD is expected at the same integration time when an anti-reflection coating is applied to the FPA.

Figure 4 shows the measured and expected mean NETDs of the FPA with various integration times. The bias voltage was adjusted to half-fill the ROIC capacitors (under 300 K background). Since the maximum bias voltage applicable by the ROIC was restricted to ~1 V, the ROIC capacitors were less than 50% filled for the integration times of 4 and 6 ms. The expected NETD was determined by using the electrical and optical characteristics of the back side illuminated variable pitch pixel arrays (flip-chip bonded to a fan-out circuit) [12]. The dashed curve (scaled $1/\sqrt{\tau}$ line) is included in the figure as a guide to the eye showing that the NETD is inversely proportional to the square root of the integration time. Since the specific detectivity of pixels is bias-independent, variation of the bias voltage does not change τ dependence of the NETD of the sensor. Therefore, the data in Fig. 4 show confirmation at the FPA level of the bias-independent specific detectivity offering great flexibility for adjusting the pixel gain (and CE) under constant sensitivity in order to adapt the FPA to different imaging conditions. It should be noted that this property of the sensor is not offered by photovoltaic detectors. There is a good agreement between the measured and expected NETDs, and the measured mean NETDs are only ~10% higher than the expected ones.

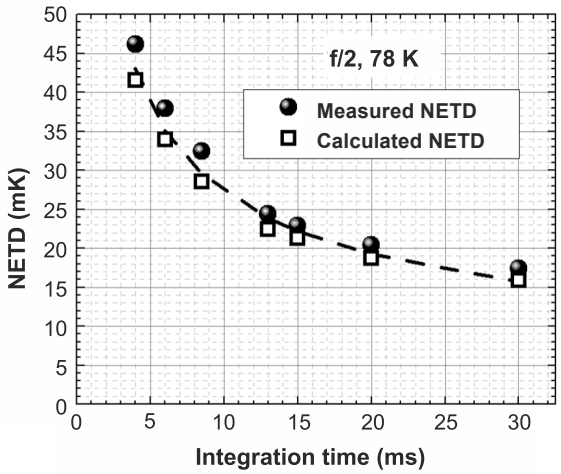

Fig. 4. Measured and expected mean NETDs of the FPA with various integration times.

A snapshot thermal image (with no frame averaging) recorded with the FPA (at 78 K, τ = 20 ms) is shown in Fig. 5 displaying a high sensitivity of the FPA. The image was recorded with the f/2.3 wide band (3–12 μm) lens.

The above characteristics of the FPA favourably compare with those of the diffraction-grating-coupled MWIR AlGaAs/$In_xGa_{1-x}As$ (low-x) [14] and $Al_{0.48}In_{0.52}As/In_{0.53}Ga_{0.47}As$ [15, 16] QWIP FPAs.

Fig. 5. A snapshot thermal image recorded with the FPA.

Gunapala *et al.* [14] reported an NETD of 17 mK for the 17.5×17.5 μm^2 pixels of a grating-coupled mega-pixel $Al_{0.3}Ga_{0.7}As/GaAs/In_{0.3}Ga_{0.7}As$ QWIP FPA with an integration time of 60 ms and f/2.5 optics at a 90 K operation temperature. High-x $InP/In_xGa_{1-x}As$ material system provides equivalent FPA performance without diffraction grating, while offering higher conversion efficiency when needed.

3. Conclusions

The two bottlenecks of the standard QWIP technology for the new generation infrared sensor technology are the need for diffraction-grating-coupling (not effectively applicable to very small-pitch sensors) and very low conversion efficiency inhibiting the successful operation of the sensor under very high frame rates and/or low background. Small-pitch (15 μm) 640×512 MWIR QWIP FPA constructed with the $InP/In_{0.85}Ga_{0.15}As$ material system exhibited an excellent NETD uniformity and low NETDs (f/2 optics) despite the absences of diffraction grating and anti-reflection coating. Therefore, a high-x $InP/In_xGa_{1-x}As$ material system, which also provides substantial conversion efficiency under moderate/large bias voltages, seems to be a proper solution to overcome the bottlenecks of the standard QWIP technology.

The epilayer structure used in this work is not optimized, and the cut-off wavelength (~6 μm) is longer than needed (5 μm) for a long-distance imaging. Therefore, there is large room for additional work to increase the background-limited operation temperature of the sensor by modifying the epilayer structure through the adjustment of the material parameters and/or utilizing low-x $Ga_xIn_{1-x}P$ barriers. It should also be noted that the present FPA provides excellent characteristics for short-distance imaging applications (which also collect photons with wavelengths beyond of 5 μm) such as medical diagnosis through thermal imaging.

Acknowledgement

The authors thank Prof. Serdar Kocaman for his contribution to this work in the flip-chip bonding of the FPA with the ROIC.

References

[1] Rogalski, A., Martyniuk, P. & Kopytko, M. Challanges of small-pixel infrared detectors: a review. *Rep. Prog. Phys*. **79**, 046501 (2016). https://iopscience.iop.org/article/10.1088/0034-4885/79/4/046501

[2] Ivanov, R. *et al*. III-V based infrared detectors are imposing new standards. *Proc. SPIE* **11407**, 114070Q-1-114070Q (2020). https://doi.org/10.1117/12.2558736

[3] Besikci, C. High-x $InP/In_xGa_{1-x}As$ quantum well infrared photodetector. *Infrared Phys. Technol*. **95**, 152–157 (2018). https://doi.org/10.1016/j.infrared.2018.10.018

[4] Peng, L. H., Smet, J. H., Broekaert, T. P. E. & Fonstad, C. G. Transverse electric and transverse magnetic polarization active intersubband transitions in narrow InGaAs quantum wells. *Appl. Phys. Lett.* **61**, 2078–2080 (1992). https://doi.org/10.1063/1.108312

[5] Karunasiri, G. *et al*. Normal incident InGaAs/GaAs multiple quantum well infrared detector using electron intersubband transitions. *Appl. Phys. Lett.* **67**, 2600–2602 (1995). https://doi.org/10.1063/1.115144

[6] Wang, S. Y. & Lee, C. P. Doping effect on normal incident InGaAs/GaAs long-wavelength quantum well infrared photodetectors. *J. Appl. Phys.* **82**, 2680–2683 (1997). https://doi.org/10.1063/1.366084

[7] Wang, S. Y. & Lee, C. P. Normal incident long-wavelength quantum well infrared photodetectors using electron intersubband transitions. *Appl. Phys. Lett.* **71**, 119–121 (1997). https://doi.org/10.1063/1.119446

[8] Ozaki, K. *et al*. Development of mid-wavelength QWIP FPA. *Proc. SPIE* **5783**, 736–746 (2005). https://doi.org/10.1117/12.603350

[9] Chou, S. T. *et al*. The influence of interface roughness on the normal incident absorption of quantum-well infrared photodetectors. *Thin Solid Films* **517**, 1799–1802 (2009). https://doi.org/10.1016/j.tsf.2008.09.066

[10] Maimon, S. *et al*. Strain compensated InGaAs/InGaP quantum well infrared detector for midwavelength band detection. *Appl. Phys. Lett*. **73**, 800–802 (1998). https://doi.org/10.1063/1.122006

[11] Besikci, C. Nature allows high sensitivity thermal imaging with type-I quantum wells without optical couplers: a grating-free quantum well infrared photodetector with high conversion efficiency. *IEEE J. Quantum Electron*. **57**, 1–12 (2021). https://doi.org/10.1109/JQE.2021.3052188

[12] Besikci, C. & Balcı, S. V. Diffraction-grating-free very small-pitch high-x $InP/In_xGa_{1-x}As$ quantum well infrared photodetectors. *IEEE Electron. Device Lett.* **43**, 1287–1290 (2022). https://doi.org/10.1109/LED.2022.3185535

[13] Cellek, O. O., Memis, S., Bostanci, U., Ozer, S. & Besikci, C. Gain and transient photoresponse of quantum well infrared photodetectors: a detailed ensemble Monte Carlo study. *Physica E Low Dimens. Syst. Nanostruct.* **24**, 318–327 (2004). https://doi.org/10.1016/j.physe.2004.06.043

[14] Gunapala, S. D. *et al*. 1024 × 1024 pixel mid-wavelength and long-wavelength infrared QWIP focal plane arrays for imaging applications. *Semicond. Sci. Technol.* **20**, 473–480 (2005). https://doi.org/10.1088/0268-1242/20/5/026

[15] Ozer, S., Tumkaya, U. & Besikci, C. Large format AlInAs–InGaAs quantum-well infrared photodetector focal plane array for midwavelength infrared thermal imaging. *IEEE Photon. Technol. Lett.* **19**, 1371–1373 (2007). https://doi.org/10.1109/LPT.2007.903338

[16] Kaldirim, M., Arslan, Y., Eker S. U. & Besikci, C. Lattice-matched AlInAs–InGaAs mid-wavelength infrared QWIPs: characteristics and focal plane array performance. *Semicond. Sci. Technol*. **23**, 085007 (2008). https://doi.org/10.1088/0268-1242/23/8/085007